POLITECNICO
MILANO 1863

SCUOLA DI INGEGNERIA INDUSTRIALE
E DELL'INFORMAZIONE

Innovative techniques for neural stimulation using magneto-electric nanoparticles

TESI MAGISTRALE IN BIOMEDICAL ENGINEERING

Tommasini Anna 10673506

Advisor:
Prof. Paolo Giuseppe Ravazzani

Co-advisors:
Giulia Suarato
Alessandra Marella

Academic year:
2023-24

Abstract: Magnetoelectric nanoparticles (MENPs) can generate locally high electric fields when activated with low-intensity magnetic fields. However, when administrated alone, MENPs can be placed randomly and tend to form clusters. The resulting, induced electric fields decay very rapidly with distance, compromising an effective tissue stimulation. In this context, the following study introduces a novel approach for tissue stimulation employing magnetoelectric nanoparticles embedded in a biocompatible 3D polymeric matrix (ME-Patch). Through an *in silico* approach, the electrical performance of the ME-Patch is optimized, starting with the implementation of a nanoscale modeling in which the materials electrical behaviors are thoroughly investigated, to reach the functional patch evaluation with a realistic peripheral nerve model. Our results offer insights for the fabrication of soft, biocompatible magnetoelectric devices capable of storing and transferring the effects of MENPs to trigger neuronal action potentials. By exploiting the ability of these novel nano-sources to wirelessly generate electricity in response to low-intensity magnetic fields, our approach holds promises for non-invasive nerve stimulation, overcoming several limitations associated with conventional stimulators and presents exciting opportunities for the advancement of neural interfacing technologies.

Key-words: magnetoelectric nanoparticles, wireless stimulation, soft biointerfaces, core-shell structures, nerve stimulation

1. Introduction

Electrical stimulation is a key therapeutic modality, based on the use of controlled electrical currents for medical interventions. It holds great promises in nerve stimulation, which is critical for restoring motor function and relieving chronic pain. However, conventional implantable devices face various challenges, including tissue incompatibility and mechanical limitations. Research is ongoing to develop advanced, biocompatible devices capable of an accurate electrical stimulation, which will eventually score a turning point in nerve tissue therapies.

The neurotechnology field studies new possibilities for interfacing the human central nervous system with innovative devices, enabling the performance of specific functions. Neuroprosthetics and electroceutics represent advanced technologies for therapeutic or assistive purposes. Combining neuroscience and biomedical engineering can address the restoration/modulation, or, in some cases, even the replacement of damaged parts of the nervous system, for example after a spinal cord injury (SCI), or following the occurrence of a neuropsychiatric disorders, a stroke, or a traumatic brain injury. Developments in sensory and motor applications have progressed for years, and some engineered strategies can be already found in clinical use, such as grasping [1], maintaining trunk posture, standing and walking, respiratory functions, controlling bladder and bowel [2]. These efforts require a new set of neural implants and the establishment of *ad hoc* neurostimulation protocols; therefore, an optimization step through computational approaches becomes imperative [3].

Specifically, neuroprosthesis include an electrical stimulator, then electrodes for stimulation, control sensors, and, optionally, an orthosis for additional movement support. There are different types of stimulation electrodes, such as implanted, percutaneous, and transcutaneous, which vary in invasiveness, selectivity, and cost. *Implanted electrodes* offer high selectivity but carry surgical risks, *percutaneous electrodes* are temporary, while *transcutaneous* ones allow immediate repositioning that makes rehabilitation faster but may have limitations for deep muscle stimulation and require higher current intensities, potentially causing undesired contractions [4].

In general, electrical stimulation (ES) is a versatile modality with various adjustable parameters to meet specific patient and treatment needs. In neuroprostheses, ES triggers action potentials in nerves by depolarizing ion channels, causing neurons to depolarize and generate action potentials. The action potentials generated travel both orthodromically and antidromically along the axon, but, in some cases, the triggered electrical signals are identical to what occurs naturally, resulting in indistinguishability at the end organ [2]. Several parameters play a key role: (i) *frequency* (optimal range: 12-50 Hz; below this interval there may be a lasting reduction in muscle strength, known as "low-frequency fatigue", while above these values the muscle strength rapidly decreases) [2]; (ii) *pulse duration*, or pulse width, which affects muscle recruitment and fatigue (shorter durations may reduce fatigue but affect muscle fiber recruitment); (iii) *amplitude* (expressed in mA), indicates the strength of the electrical current administered (higher amplitudes may lead to greater depolarization of the structures underlying the electrodes, contributing to greater gains in muscle strength, lower intensities may activate the central nervous system more); (iv) *electrode placement* and (v) *stimulation intensity* [5].

Nanomedicine is the branch of medicine that explores nanotechnology strategies for therapeutic and diagnosis purposes. Recently, researchers in this field have turned their scientific interests toward magnetoelectric nanoparticles (also known as MENPs), thanks to their unique features [6], [7]. In contrast to traditional nerve electrodes classified as invasive, with limited spatial resolution and poor efficiency of stimulation, magnetoelectric nanostructures may offer a wireless approach and a strong capability to produce high electric field levels in their proximity [8]. Thus, these nanostructures represent a promising avenue for biotechnology considering that they allow the modulation of significant responses which can be exploited for several biological functionalities, such as precise control of drug delivery [9], activation of biological mechanisms, advancement in the tissue engineering field [10], and facilitation of cellular manipulation [10], [11].

Nanoparticles are typically designed as core-shell structures, as shown in Fig. 1, to ensure transmission of the pressure generated by the core deformation and exerted onto the piezoelectric shell [12].

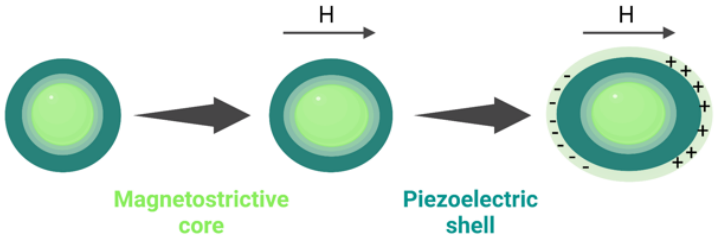

Fig. 1 Electric Field generated in response to the applied magnetic field.

Compared with other nanoparticles, MENPs have a distinctive feature, namely the presence of the magnetoelectric (ME) effect. This property enables the combination of intrinsic electric fields at the nanometric level as a result of the application of external, low-intensity magnetic fields, thus providing an efficient wireless control. As a result of the application of a magnetic field, the dipoles of the magnetostrictive core orient themselves with the force lines of the field causing it to deform. The strain is absorbed by the shell in the form of pressure, and this mechanical stimulus is converted into electrical energy, thus generating a local electric field. The correlation between magnetic and electric fields can be formulated through the Landau theory [13], which expresses their coupling by the magnetoelectric coefficient $\boldsymbol{\alpha}$**ME,** defined with the following equation:

$$\boldsymbol{\alpha_{ME}} = p \times \lambda = \frac{\Delta E}{\Delta S} \times \frac{\Delta S}{\Delta H} = \frac{\Delta E}{\Delta H} \left[\frac{V}{cm\ x\ Oe} \right]$$

where p and λ are the piezoelectric and magnetostrictive coefficients, respectively; ΔE is the change in the electric field due to the ME effect, ΔS is the variation in strain from the magnetostrictive core deformation, and ΔH is the applied magnetic field [14]. Thus, polarization can be induced through the application of a magnetic field, and, reciprocally, magnetization can be induced through the application of an electric field, working in either direct or inverse modes [6].

Configurations vary according to the size, shape, interface coupling of the ferromagnetic (FM) and the piezoelectric (PE) phases. These include two-phase composites, with ferromagnetic and piezoelectric particles immersed in a neutral matrix, ferromagnetic particles dispersed in a piezoelectric matrix, or again with ferromagnetic rods immersed in a piezoelectric matrix. In addition, there are planar composites, with alternating layers of ferromagnetic and piezoelectric materials, and core-shell nanocomposites, with a ferromagnetic core and a piezoelectric shell. The choice of structural configuration depends on the specific needs of the application and can be optimized to achieve certain desired properties and performance [15].

Bottom-up methods are used to synthesized MENPs such as hydrothermal [16], sol-gel [17], solvent evaporation, and solid-state reactions. Among these, sol-gel and hydrothermal methods are the most widely used, leading to the synthesis of uniform core-shell structures with controlled morphologies [14]. Starting with a magnetostrictive material, capable of converting a magnetic field into a strain, a piezoelectric material is coupled, which converts the generated strain into an electric field. A commonly used composite is formed by combining $CoFe_2O_4$ (cobalt ferrite, CFO) for the core, and

$BaTiO_3$ (barium titanate, BTO) for the shell. The resulting composite material shows excellent biocompatibility and significant magnetoelectric coupling coefficient, which remains considerable even at room temperature [14], [15].

Few, recent studies have assessed the use of MENPs *in vivo*. Typically, magnetoelectric nanoparticles are injected into specific anatomical targets [18], [19], and can generate highly focused electric fields (in the order of 10^5 V/m) [8], approaching the threshold of neural activation. Despite the significant advantage of a very focused distribution, the electric fields generated decrease rapidly at distances of a few millimeters from the MENPs positioning [8]. Due to their broad potentialities, MENPs could also be integrated as innovative electromagnetic field-based tools for the development of biohybrid interfaces that facilitate interconnection between living and artificial systems.

In the early stages of the design of novel medical devices for neurostimulation, it could be advantageous to rely on the use of computational modeling to assess the device properties and solve the bioelectromagnetic problems. The computational approach makes it possible to replace or reduce the requirement and costs associated with experimental studies (*in vitro* and *in vivo*), offering a predictive approach, of primary importance at the early stages of the design of novel therapeutic strategy. This in silico preliminary, yet essential, characterization allows to sustain the 3Rs principle, reducing the amount for future animal experiments, improving the quality of research and optimizing the use of available resources. A wide range of electrical phenomena and the resulting neuronal responses can be predicted by adopting advanced *in silico* tools, allowing to screen a wide ranges of configurations, parameters and operating conditions. Only the best configurations will be then translated to future *in vitro* and *in vivo* experimental studies.

Leveraging on previous research results on magnetoelectric nanoparticles (MENPs) and considering the increasing demand for flexible and functional biointerfaces, our project aims to develop an innovative method to generate magnetoelectric stimuli. The goal is to incorporate CFO-BTO MENPs into a soft, biocompatible polymer matrix to overcome limitations related to the rapid spatial decay of electric fields produced by single nanoparticles or small aggregates of MENPs, which may compromise an effective tissue stimulation. Our approach aims to create a clinically usable size structure that can be mechanically adapt to specific requirements and reach the excitation threshold of peripheral nerves. In our three-dimensional computational model, the electrical properties of the polymer are initially modified to study the electrical output of the designed magnetoelectric patch (ME-patch) within a biological nervous environment; once the nanoscale configuration is optimized, a micrometric patch is constructed, to evaluate the actual electric field distribution in a realistic model of human peripheral nerve. Lastly, a millimetric model is implemented for a conclusive analysis of the response in terms of neuronal dynamics generated by the magnetoelectric electrode. The use of advanced computational models through solvers combining finite element method (FEM) and neuronal dynamics is useful for studying this scenario. The findings of our complex and detailed computational framework represent an important step toward the development of innovative therapies to treat neurological disorders and restore impaired neuronal function.

2. Material and methods

In this study, the methodology used to evaluate the feasibility and functionality of the MENPs-based composite patch on peripheral nerve stimulation can be summarized through three major steps, as described by the flowchart in Fig. 2.

Sim4Life software (ZMT Zurich Med Tech AG, Zurich, Switzerland, www.zurichmedtech.com) was adopted to model the electric field interaction with the human body. This allows a precise modeling and analysis of the effects of electromagnetic field (EMF) exposure on biological systems.

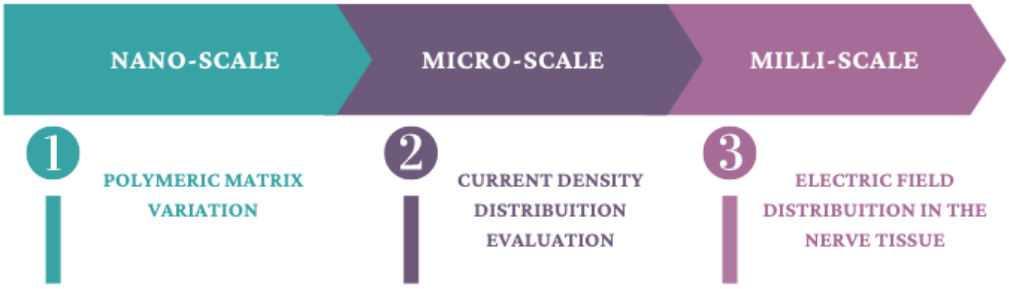

Fig. 2 Simulations Step Flowchart.

In the first phase of the study, simulations were conducted on MENPs-functionalized polymeric grafts at the nanoscale, by considering a nanometric unit. These composite structures were virtually embedded within a cubic environment presenting the dielectric properties of the nerve tissue to evaluate the potential of three different materials to act as sources of the electric field resulting from the MENPs magnetoelectric phenomenon.

Subsequently, an intermediate micrometer-scale structure is introduced, placed within a cubic geometry that mimics the electromagnetic properties of the nerve tissue. This step focuses on the maintenance of a dipole behavior and current density distribution by increasing the size of the composite graft, to sustain the transition to the millimeter scale, described in the next step.

In the third and final chapter, the millimetric model is presented. The electric field generated in the surroundings of the real nerve model, imported from the software library, was examined. As a concluding part of the work, a specific software environment named Neuron is used, enabling the translation of the obtained electromagnetic results into action potentials and hence into neuronal electrical responses.

2.1 Nanometric structure

The nanometer unit is the fundamental element, which is ideally replicated to form the millimetric clinically-size structure. Several simulations were conducted considering three different polymers: the electrical features of the whole composite patch were evaluated based on the dielectric properties of the polymeric matrixes. Particular attention was given to the analysis of the electric potential and current density profiles at the volume surface.

2.1.1 MENP model and Electromagnetic simulation settings

Sim4Life was the used platform, and it resolves the low-frequency electromagnetic problem using the ohmic quasi-static approximation, a numerical technique within the finite element method (FEM). This approach is particularly useful for solving partial differential equations in complex geometries where analytical methods are impractical. Through FEM, the Laplace equation used to obtain the electric potential (ϕ) becomes: $\nabla \cdot (\sigma \nabla \phi) = 0$. Where σ (S/m) is the electrical conductivity of tissues set according to the stimulating frequency. Following previous research works, the chosen frequency is 100 Hz, which is commonly adopted for neural stimulation studies, as reported in the literature [19]. Then, the E field distribution was derived by means of the following relation: $E = -\nabla \phi$. The model consists of three different subdomains: (i) the 3D MENPs; (ii) the polymer matrix

represented by a cubic volume of side 400 nm; (iii) the surrounding tissue of cubic geometry of side 800 nm.

Considering previous studies on MENPs regarding the optimal range of sizes and shapes [20], a spherical structure with a diameter of 90 nm was chosen for this study. The magnetoelectric effect occurs in the presence of a low-amplitude magnetic field and is followed by the generation of an electric potential on the surface of the nanoparticles whose distribution exhibits a dipolar configuration. To represent this feature, it is necessary to assume a parameterization i.e., modeling them through two hemispheres, as shown in Fig. 3, one with a positive electric potential of +2.25 mV and one with a negative potential of -2.25 mV; the above settings are imposed via Dirichlet boundary conditions chosen based on previous analyses conducted with COMSOL Multiphysics® 5.6 (www.comsol.com). The insulating layer between the two caps is constituted of Tecothane 75D ($V = 0$, $\sigma = 0$, $\varepsilon = 3.4$ and $\mu = 1$), whose dielectric properties were assigned by the software library [21] and automatically adjusted according to the stimulation frequency.

The adopted nanometer unit has a cubic polymer matrix with a side of 400 nm, containing six MENPs. Four of these particles are positioned on the plane of symmetry of the cubic structure, while the other two are located outside this plane and all at 120 nm from each other, as shown in Fig. 3. This arrangement ensures a uniform distribution in space, avoiding unwanted overlapping and maximizing the magnetoelectric effect of the nanoparticles.

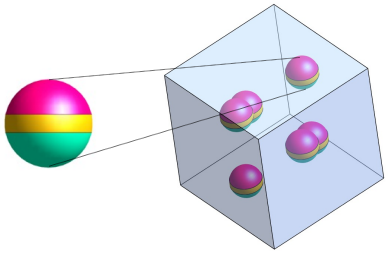

Fig. 3: MENP model in Sim4life Green shell with V= - 0.00225 V, Pink shell with V= + 0.00255 V, and middle layer Tecothane 75D material in yellow.

Next, the obtained nanoscale composite was embedded within a cubic domain of larger dimensions, whose electrical properties are associated with the nerve tissue feature, predefined in the materials database and directly integrated into the software ($\sigma = 3.48 \times 10^{-1}$, $\varepsilon = 466016$, and $\mu = 1$) [21].

Three different simulations were conducted, by varying the polymeric matrix. The polymers considered are: polycaprolactone (**PCL**), poly(3-hexylthiophene) (**P3HT**) and a mixture of silk fibroin and polypyrrole (**SF-PPy**), whose electromagnetic properties are listed in Table 1.

Table 1: Electrical and mechanical properties of the polymeric materials under study

	Density [kg/m³]	***Electrical Conductivity [S/m]***	***Relative permittivity***
PCL	1.14×10^3	1×10^{-6}	2.84
P3HT	1.15×10^3	2.24×10^4	3
SF-PPy	1.14×10^3	80	6.1×10^{-6}

For each nanometric unit considered, a qualitative evaluation of the potential and the current density at the polymer surface was carried out, followed by a quantitative analysis of the statistical parameters via Matlab R2023b and OriginPro2022.

2.2 Micrometric structure

Once the optimal material is identified from those previously analyzed, a transition to a micrometer structure was performed. The nanometer model acts as basic unit, and it gets replicated on a large scale to generate a micrometric-sized patch. Since the goal is to study the behavior of the full-scale structure based on nanosources, the implementation of an intermediate structure facilitates the transition from the nanoscale to the millimetric one.

2.2.1 Micrometric model and Electromagnetic Stimulation Settings

In this step of the thesis, two models were designed by bringing together three and four fundamental units in each spatial dimensions, for a total of 27 and 64 base units, respectively. The resulting microstructures have a cubic shape with sides of 1.2 μm and 1.6 μm, within which 165 and 384 MENPs are distributed, respectively. Similarly to the nanometer model, the micrometer-sized patches are contained in a larger volume, in this case presenting a side of 2 μm, as depicted below, in Fig. 4:

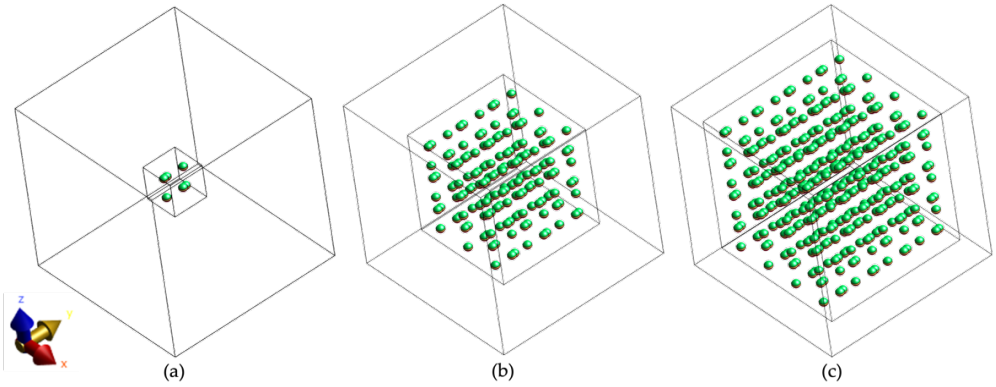

Fig. 4 Micrometric Patch modelled in Sim4life. MENPs are depicted in green and are encapsulated in the polymer matrix (inner box); (a) the model of the nanometric unit with sides of 0.4 μm and 5 MENPs; (b) the microstructures with sides of 1.2 μm and 165 MENPs and (c) the microstructures with sides of 1.6 μm and 384 MENPs.

The low-frequency electromagnetic stimulation involves the same settings established for the initial phase. At a stimulation frequency of 100 Hz, a comparison between the nanometric basic unit (Fig. 4a) and the two microstructures (Fig. 4b and 4c) was carried out. Specifically, distributions of current density and electrical potential developed at the surface of the models were studied.

2.3 Millimetric structure

To allow for an easier transition from the nanometer model to the millimeter model, a simplifying hypothesis was adopted that assumes for both models the same basic scheme. To build the millimeter model, the volume fraction of 0.04 and the scaling factor were considered, using which the radius of the magnetoelectric nanoparticles in the millimeter unit and their distance from each other were determined.

This simplification allows to overcome the computational constraints of the software, which does not support calculations with a high number of base units. Consequently, the millimeter model was

shaped ensuring consistency with the real phenomenon by maintaining constant current density values at the surface.

2.3.1 Nerve Model and Electromagnetic Stimulation Settings

Sim4Life provides a powerful modeling environment, enabling the management of complex anatomical models, such as ViP and CAD models. Virtual Population ViP3.0 mockups, advanced computational human phantoms, are ideal for mechanical studies, medical device testing, and clinical trial integration. There are also specific organ models to meet anatomical accuracy requirements. For this study, a cylindrical nerve model, as shown in Fig. 5a, was imported to ensure accurate representation of actual proportions in relation to the millimetric electrode.

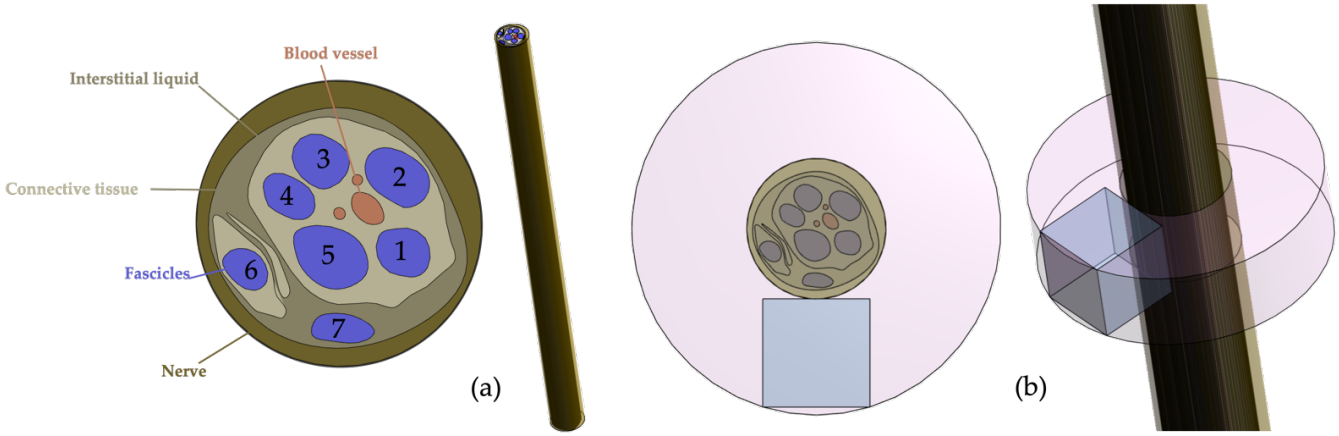

Fig. 5 (a) Cross section of nerve model and its entire view; (b) cross section of millimeter model adopted in the study and its default view.

The nerve model consists of subdomains representing the different tissues, each of which has different electrical characteristics updated independently with respect to the stimulation frequency. Table 2 shows the electrical characteristics of the tissues based on the frequency applied in this work.

Table 2 Electric Properties of tissues in the nerve model

Tissues	*Electrical Conductivity [S/m]*
Nerve and Interstitial	*0.28*
Connective	*0.38*
Fascicles	*Anisotropic (xx, yy, zz): 0.088, 0.088, 0.5*
Blood	*0.66*

The designed soft ME-patch was placed in contact with the nerve model and encapsulated in a silicone construct, as shown in the previous Fig. 5b. This configuration was adopted to ensure consistency with previous models in the software tutorials. In the simulations, that material was used because it exhibits a significantly lower electrical conductivity value than the other materials employed ($\sigma = 1 \times 10^{-12}$ *S/m)*, due to isolate the electrode from its surroundings and ensure that electrical charges are conveyed to the nerve fibers.

Staying with electromagnetic simulations, for this model electric field distributions within the nerve cross section were investigated. In support of the qualitative results, the plot of the electric field decay as the distance from the patch increases is plotted, considering the various configurations assumed by the patch and the different electrical properties presented by different tissues.

2.3.2 Nerve Model and NEURON Stimulation Settings

The computational simulation platform Sim4Life is equipped with the NEURON solver, an environment for implementing biologically realistic models of electrical signaling in individual neurons. It simulates the equations that describe nerve cells, known as the wire equations, and solves them computationally. Every fascicle Fig. 6c, blue element in Fig. 6a, is composed of four fibers (also named "splines" Fig. 6d-e) each having a diameter of 5.7 µm and a length of 17,5 µm. In this study, among the various nerve models in the software, the MOTOR type was adopted, which is the most representative of human arm nerve behavior. The equivalent circuit is shown in Fig. 6g, and it includes explicit representations of Ranvier's nodes, paranodal and internodal sections of the axon, and a myelin sheath with finite impedance.

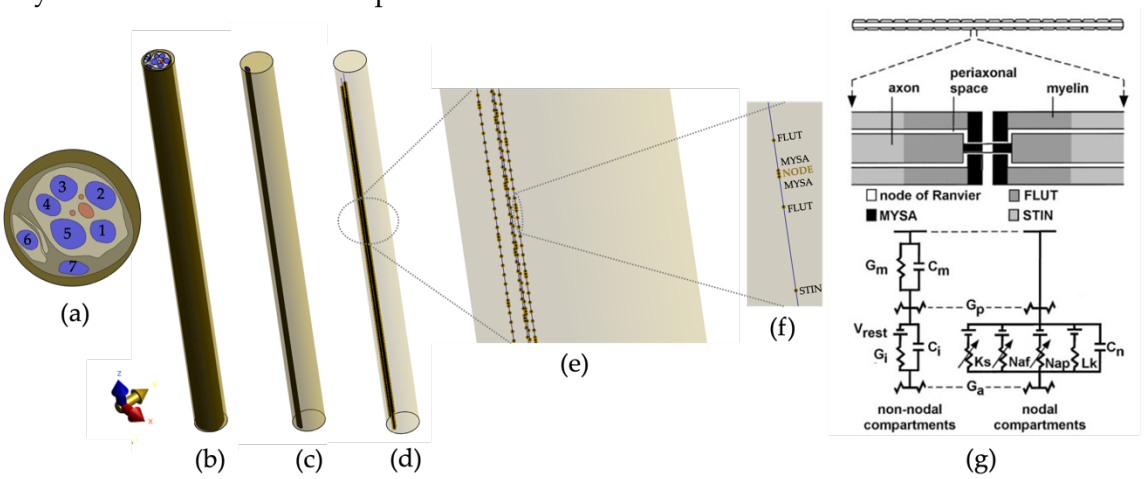

Fig. 6 (a) Cross section of Nerve model imported from the software libraries; (b) Nerve model from longitudinal view; (c) The Nerve model is composed by 7 fascicles; (d) Each fascicle is composed by 4 fibers named splines; (e) The MOTOR model defined a spline of length 17,5 µm as a sequence of 34 nodes and 33 internodes ; (f) Zoom of a single spline divided in nodes and internodes (STIN, FLUT, MYSA); (g) Electrical equivalent circuit of nerve model.

The MOTOR model consists of 34 nodes of Ranvier separated by 33 internodes for the splines of the model whose length is 17,5 µm. This model is focused on the axonal process which is composed of 11 compartments: two myelin attachment segments (MYSA), two paranode main segments (FLUT), six internode segments (STIN), and node of Ranvier (NODE). Nodal membrane dynamics includes in parallel: fast (*Naf*) and persistent (*Nap*) conductances for sodium and slow for potassium (*Ks*); which describe the behavior of the respective voltage-gated ion channels present in the portion of the cell around Ranvier's node. In addition to these, there is also a linear leakage conductance (*Lk*) that represents the behavior of the other channels present in the node; all conductances are paralleled with the nodal capacitance (*Cn*) which describes the accumulation of electrical charge at the membrane [22]. By the accurate representation of ion channels in the node, double-cable representation is necessary to represent the geometry of the nerve axon and so the internodal segments. They consist by linear conductances with an explicit representation of the myelin sheath (*Gm* in parallel with *Cm*), an insulating coating which accelerates the transmission of nerve impulses and the internodal axolemma (*Gi* in parallel with *Ci*), the cell membrane, composed mainly of phospholipids, proteins and carbohydrates [23].

2.3.3 Stimulation Settings

The NEURON solver uses as input the electric field values obtained from previous electromagnetic simulations. Modeling based on the human nerve allows an accurate approximation of the electrical response of a peripheral nerve located near the structure.

The pulse used to stimulate the nerve is defined as a sine wave of 50 periods and with an amplitude equal to that of the electric fields obtained in previous simulations. The duration and time step are 500 ms and 0.0025 ms, respectively.

Starting from the electromagnetically analyzed configurations, only some simulations are run, those in which there is a slower decay of the electric field. For each simulations, the nerve responses of spline 0 fascicle 7 (Fig. 5b), which is the one closest to the patch, are evaluated; to further explore the concept of deep stimulation, the nerve responses of spline 2 fascicle 5 and spline 0 fascicle 3 (on axis with spline 0 of fascicle 7 but located gradually farther away from the patch) (Fig. 6a), are explored.

3. Results

3.1 Nanometric structure

In the first part of this thesis, the electric potential profile of the MENPs-polymer composite was evaluated, to determine the effect of the nanoparticle activation on the overall patch behavior. The analysis was performed varying the matrix polymer, as shown below (Fig. 7). The study adopts biocompatible materials suitable for various biotechnological applications, either of synthetic origin, such as polycaprolactone (PCL), poly(3-hexylthiophene) (P3HT), or naturally-derived materials, such as the silk fibroin-polypyrrole (SF-PPy) blend, thus covering a wide range of electrical conductivity values ($\sigma_{PCL} = 1 \times 10^{-6}$ S/m, $\sigma_{SF\text{-}PPy} = 80$ S/m, $\sigma_{P3HT} = 2.24 \times 10^{4}$ S/m).

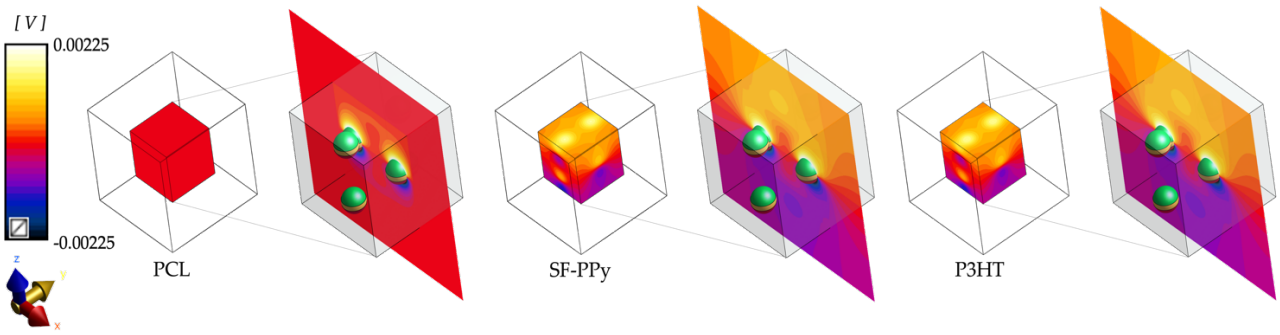

Fig. 7 Electric Potential profiles in the three different MENPs-polymers composites under study (polycaprolactone (PCL), poly(3-hexylthiophene) (P3HT) and a mixture of silk fibroin and polypyrrole (SF-PPy). The cross-section on place xz represents the center of the ME-patch.

Subsequently, the resulting current density at the nanometric patch surface was observed, taking both a qualitative (Fig. 8) and quantitative approach (Table 3), to assess qualitative variations in the electrical behavior when the three polymers are used as matrix material for the MENPs accommodation.

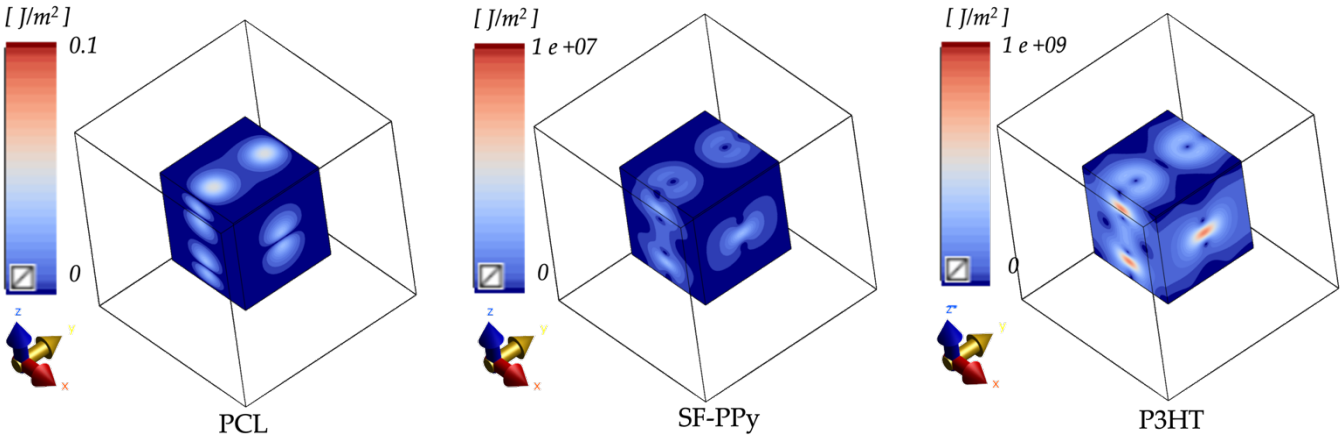

Fig. 8 Current Density profiles at the magnetoelectric patch surface, in the three different MENPs-polymers composites under study (polycaprolactone (PCL), poly(3-hexylthiophene) (P3HT) and a mixture of silk fibroin and polypyrrole (SF-PPy).

The outcomes of the statistical analysis conducted on the various current density profiles are reported in Table 3, while the values distributions are graphically represented by means of box plots (Fig.3), which allow a more intuitive visualization of the variations in the data. Goal of this comparison was the choice of the optimum polymer matrix – MENPs combination, being the most conductive one the most promising for our envisioned application.

Table 3 Statistical analysis on different adopted polymers (polycaprolactone (PCL), poly(3-hexylthiophene) (P3HT) and a mixture of silk fibroin and polypyrrole (SF-PPy)).

J [A / m²]	**PCL**	**SF-PPy**	**P3HT**
Mean	3.04×10^{-2}	7.66×10^{3}	1.22×10^{8}
Median	2.16×10^{-2}	4.52×10^{3}	8.29×10^{7}
Maximum	1.41×10^{-1}	3.91×10^{4}	8.13×10^{8}
Minimum	2.22×10^{-4}	7.69×10^{1}	4.54×10^{5}

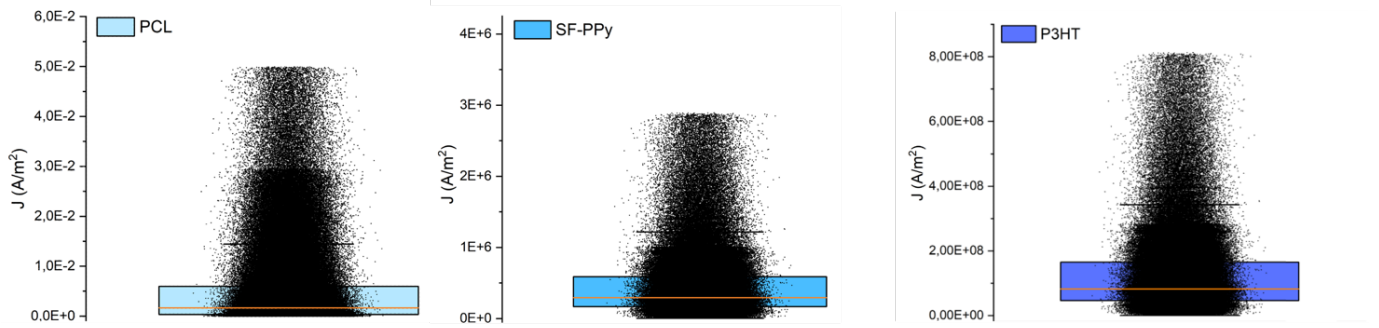

Fig. 9 Boxplot of current density of the different polymers

3.2 Micrometric structure

In the second part of this project, the analysis is further expanded by focusing on the construction of a micrometer structure, which is composed of multiple nanometer units. The investigation

conducted at this stage is performed by adopting the most conductive polymer (i.e., the P3HT). The two micrometer models are analyzed with respect to the nanometer model. These incorporate three and four basic units in each spatial dimension, for a total of 165 and 384 MENPs contained, respectively. To understand how the collective behavior affects the overall electrical performance, the electric potential distribution is visualized in Fig. 10 below.

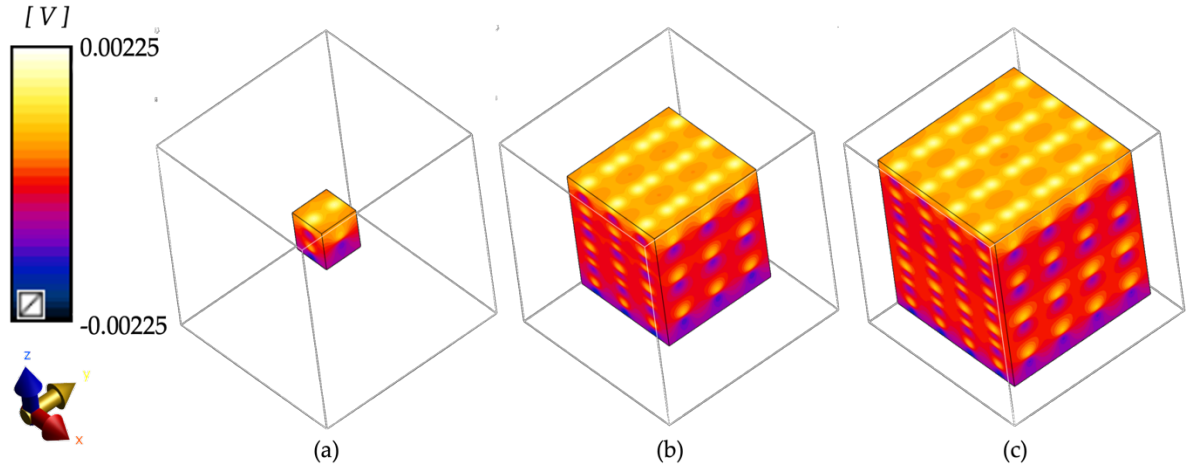

Fig. 10 Electrical Potential distribution at the outer surface of the ME-patch: (a) nanometric model (1 base unit, 6 MENPs); (b) 1.2 μm side structure (27 base units, 162 MENPs); (c) 1.6 μm side structure (64 base units, 384 MENPs).

For supporting the accomplished qualitative analysis, a statistical analysis is performed on each face of the 1.6-μm side structure and reported in Table 4, considering the spatial symmetry of the six faces.

Table 4 Statistical analysis of the electric potential distributions with respect to each of the six faces of the 1.6 μm side micrometric structure (Fig. 10c).

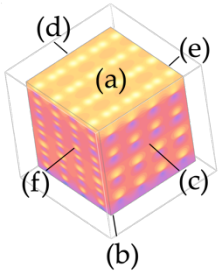

ϕ [V]	(a)	(b)	(c) & (d)	(e) & (f)
Mean	$9{,}05 \times 10^{-4}$	$-9{,}20 \times 10^{-4}$	$-5{,}20 \times 10^{-6}$	$-5{,}16 \times 10^{-6}$
Median	$7{,}99 \times 10^{-4}$	$-8{,}15 \times 10^{-4}$	$-5{,}23 \times 10^{-6}$	$-4{,}79 \times 10^{-6}$
99th percentile	$1{,}71 \times 10^{-3}$	$-1{,}71 \times 10^{-3}$	$9{,}28 \times 10^{-4}$	$8{,}50 \times 10^{-4}$
100th percentile	$1{,}76 \times 10^{-3}$	$-1{,}77 \times 10^{-3}$	$1{,}33 \times 10^{-3}$	$1{,}00 \times 10^{-3}$

In addition to visualizing the potential distribution, the current density profiles between the nanometer unit and the two micrometer structures are displayed in Fig. 11. Again, the mean, median, maximum and minimum values of the entire surfaces of the structures were investigated in detail and reported in Table 5.

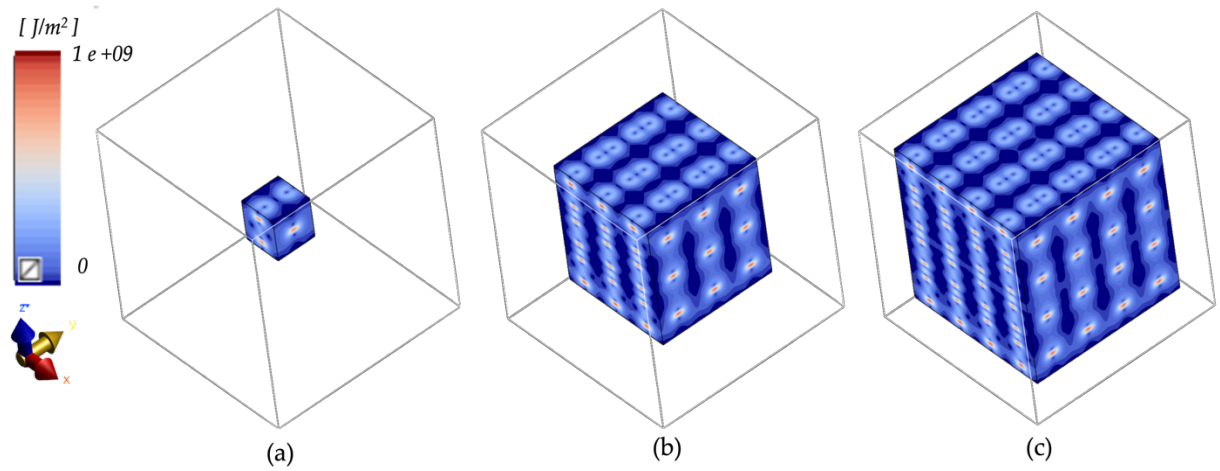

Fig. 11 Current Density distributions at the outer surface of the ME-patch: (a) nanometric model (1 base unit, 6 MENPs); (b) 1.2 μm side structure (27 base units, 162 MENPs); (c) 1.6 μm side structure (64 base units, 384 MENPs).

Table 5 Statistical analysis on the current density profiles for the different modelled structures

***J* [A / m²]**	400 nm	1.20 μm	1.60 μm
Mean	1.22×10^8	1.16×10^8	1.19×10^8
Median	8.29×10^7	7.77×10^7	7.94×10^7
Maximum	8.13×10^8	8.90×10^8	9.67×10^8
Minimum	4.54×10^5	1.11×10^6	4.77×10^5

3.3 Millimetric structure

Overcoming the limitations of the computational tool that impairs the true modeling of the millimeter system, the simplification of keeping the nanometer model even for the millimeter is adopted. A trial-and-error approach is taken to calculate the appropriate potential to be applied to the nanoparticles in the millimeter model. This potential (Table 6: *bold* value) shall be capable to generate a current density (Table 6: value in *blue*) comparable to that observed in the nanometer structure (Table 6: value in *orange*), demonstrated through the results in the micrometer structure section to be maintained regardless of the increasing number of nanometer units within the structure.

Table 6 Electric potential values explore in the Trial & Error experiment; the orange value indicates the median of the current density on the surface of the nanometric structure; the value in blue represents the median of the current density on the surface of the millimetric model which best fits with the behavior of the nanometric structure; the bold value in the header row of the table indicates the potential value to be imposed on the nanoparticles of the simplified millimetric model.

***J* [A / m²]**	**nanometric**	5 V	5.5 V	5.2 V	**5.25 V**	5.3 V	6 V
Mean	1.22×10^8	1.15×10^8	1.27×10^8	1.20×10^8	1.21×10^8	1.22×10^8	1.39×10^8
Median	**8.29×10^7**	7.84×10^7	8.63×10^7	8.16×10^7	**8.23×10^7**	8.31×10^7	9.41×10^7
Maximum	8.13×10^8	7.94×10^8	8.73×10^8	8.25×10^8	8.33×10^8	8.41×10^8	9.52×10^8
Minimum	4.54×10^5	4.93×10^5	5.43×10^5	5.13×10^5	5.18×10^5	5.23×10^5	5.92×10^5

A scatter box blot is developed to compare and validate the distribution of the point data obtained.

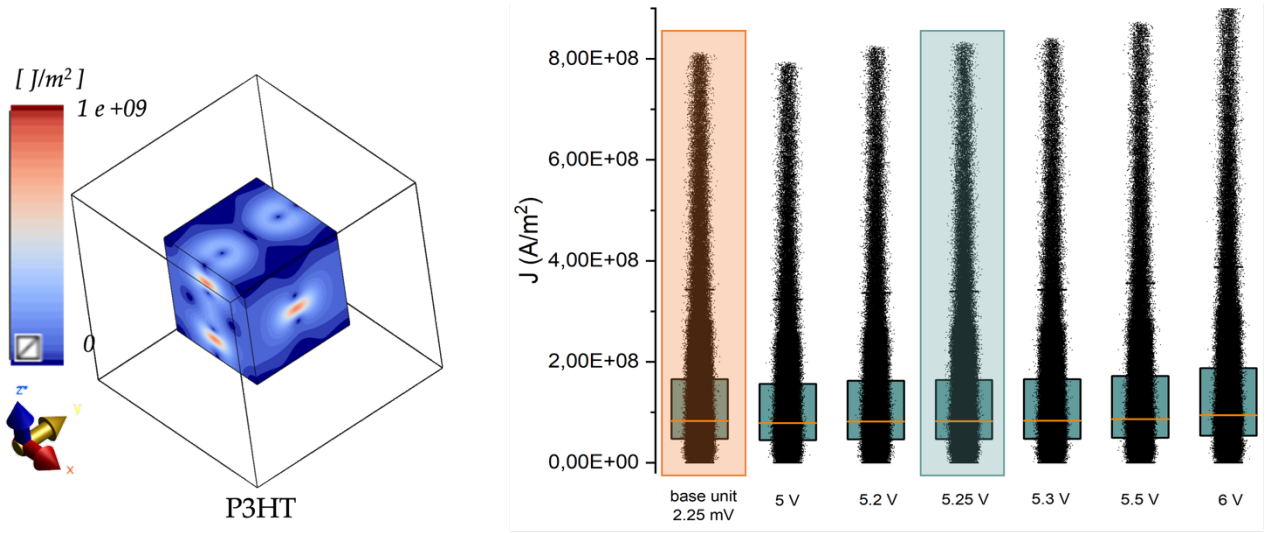

Fig. 12 On the right: Scatter box plot for finding the potential to be imposed on MENPs in the millimetric-size patch; the box in orange indicates the distribution of current density values on the surface of the nanometer structure; the box in blue represents the distribution of current density values on the surface of the millimeter model with a potential of 5.25 mV, the set up that best fits the behavior of the nanometer structure.

3.3.1 Nerve Model and Electromagnetic Stimulation

Observing the current density values on the surface of the millimeter structure, three different distributions of this parameter can be appreciated, which occur on opposite faces of the cubic volume. Six simulations are conducted and presented, arranged in pairs. Each pair represents an electrode face oriented differently with respect to the longitudinal axis of the nerve (in Fig. 13 (i): A – B, (ii): C – D and (iii): E – F).

The electric field distributions in the cross section of the nerve are reported in Fig. 13, thus understanding and analyze how the different orientations behave in terms of the field generated and how this is felt within the biological environment, consisting of different tissues with their respective electrical characteristics.

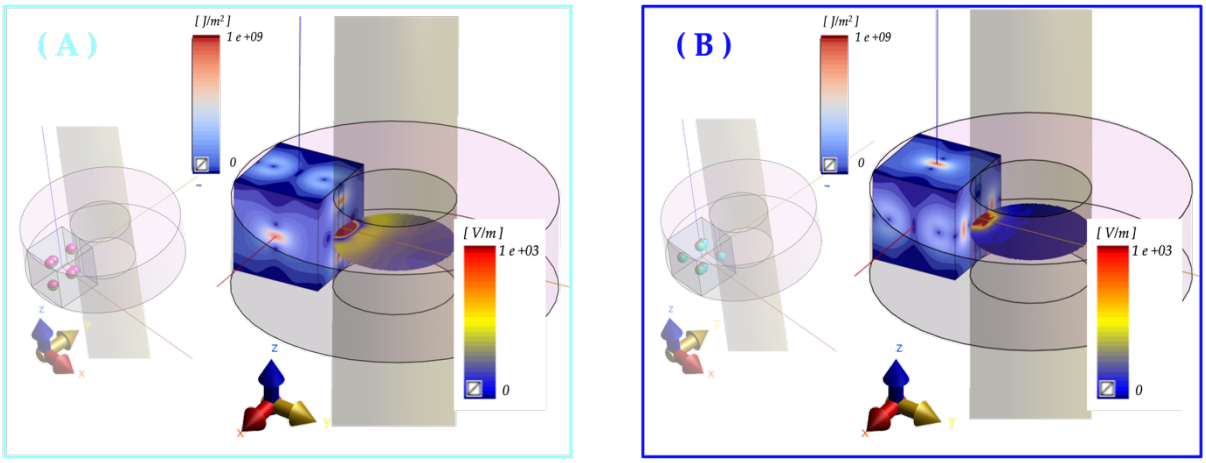

(i)

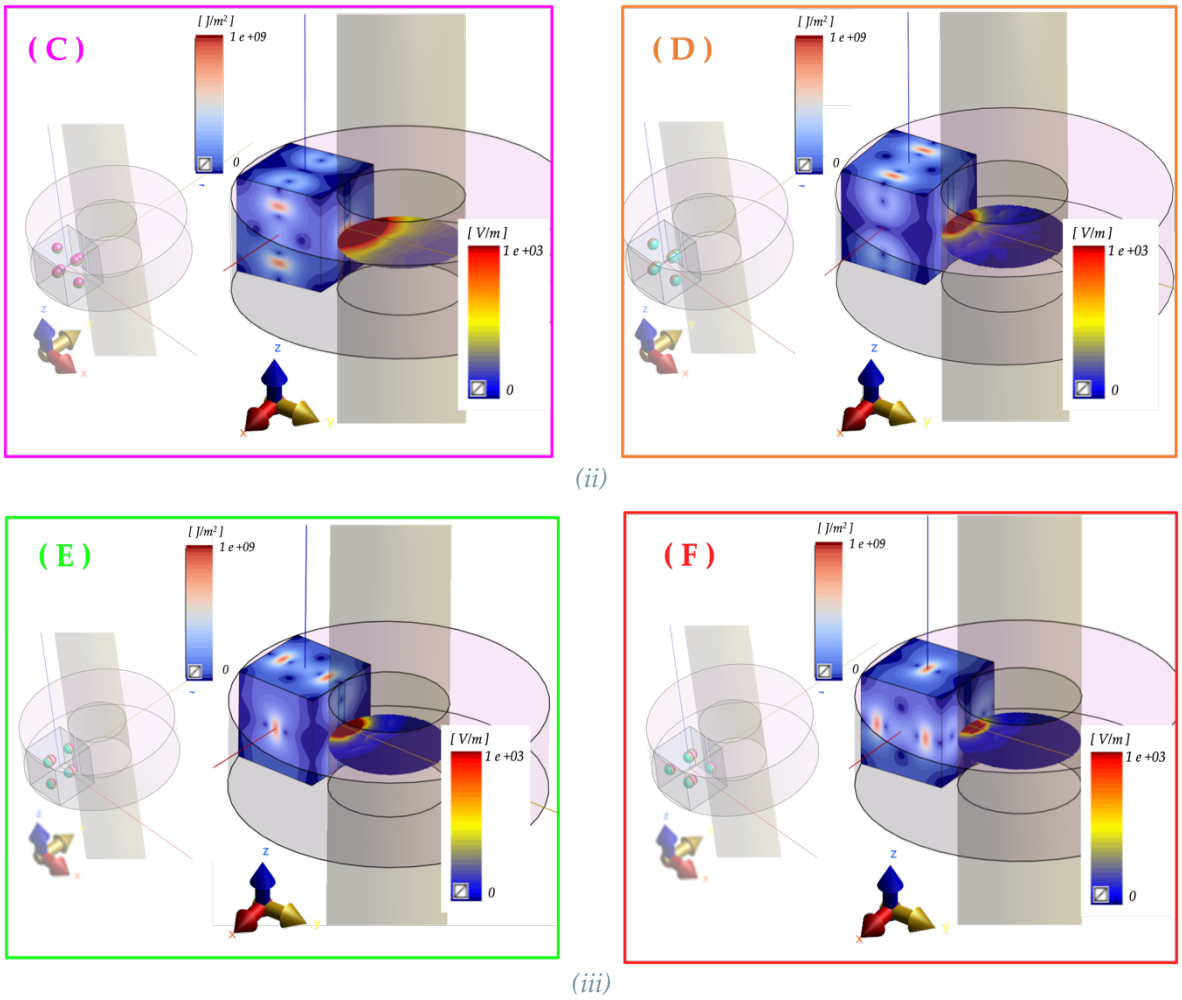

(ii)

(iii)

Fig. 13 Six different electromagnetic field profiles organized in pairs. Each ones represents an electrode face oriented differently with respect to the longitudinal axis of the nerve.

Considering the changes in the electric field, the concept of field penetration is explored. The electric field profile in the transversal section of the nerve is plotted by comparing the two orientations of the same current density face. In the figures below, the full decay profile is presented and a zoom with 0-300 V/m range to accurately visualize what happens when progressively moving away from the ME patch.

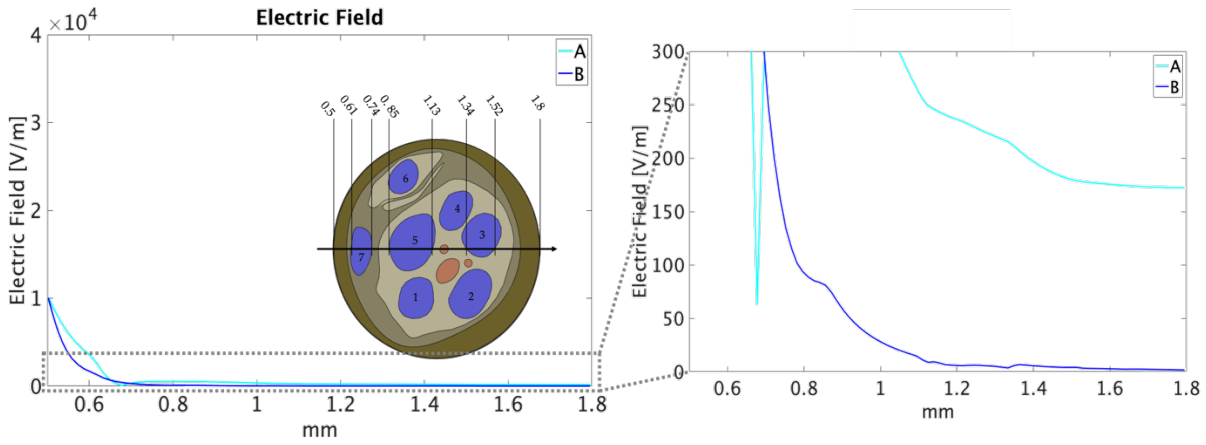

(i)

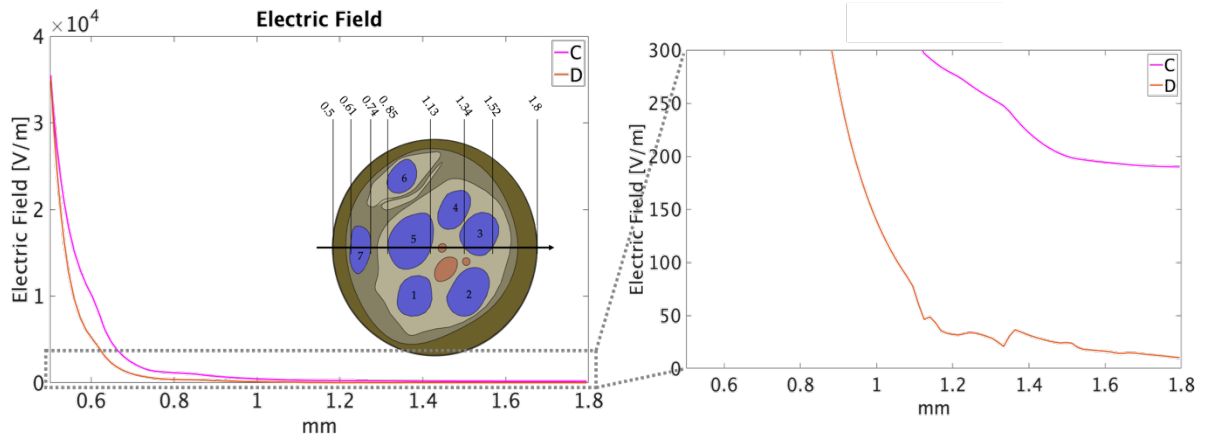

(ii)

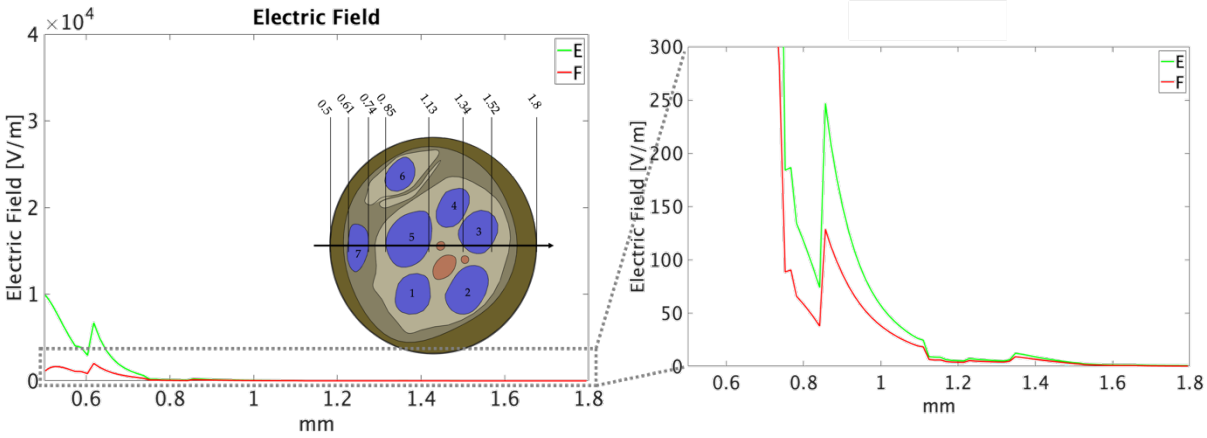

(iii)

Fig. 14 Comparison of the spatial decay of the six electromagnetic simulations organized in pairs, with their respective zooms [0-300 V/m]. Each pair shares the same ME-Patch face oriented differently with respect to the longitudinal axis of the nerve: (i) simulations A and B; (ii) simulations C and D; (iii) simulations E and F.

3.3.2 Nerve Model and NEURON Stimulation

Neuronal dynamics is studied via Neuron, which uses as input the electric field values obtained from previous electromagnetic simulations. By coupling the electromagnetic field stimulation with the solver, it is possible to observe the neuronal dynamic response. For each of the three pairs, the pairwise configuration promising slower decay is considered (A, C, and E in Fig. 13). APs related to the neuronal response of fascicle 7, defined as the one closest to the electrode (cross section of the nerve in Fig. 5a), are analyzed. For each, the concept of deep stimulation is explored in depth; to this end, action potentials related to fascicles 3, 5, and 7 were plotted (cross section of the nerve in in Fig. 5a); These fascicles are gradually distant from the electrode and, consequently, were affected differently by the electric field generated by the patch-ME.

Presented in the following Fig. 15 are: on the *left*, the APs in fascicle 7 for the most promising configurations among each of the three pairs and, on the *right*, the APs of a spline in fascicle 5 and fascicle 3 in comparison to that in fascicle 7.

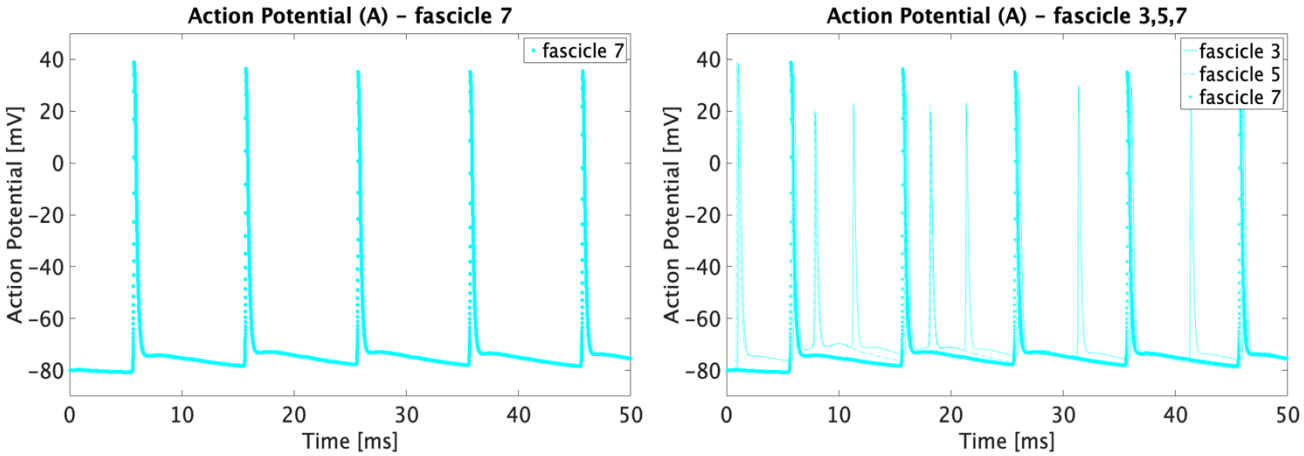

(i)

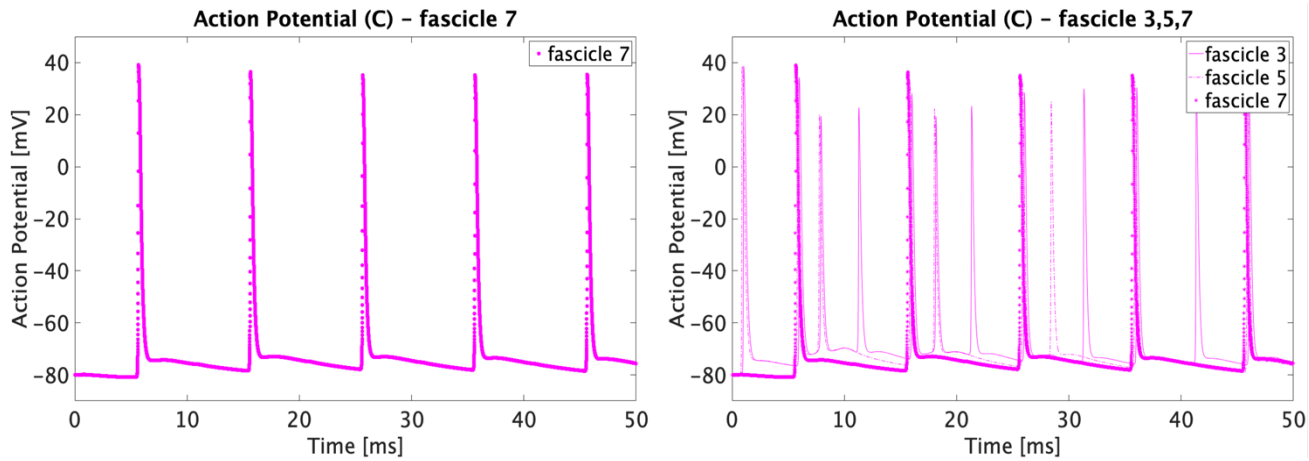

(ii)

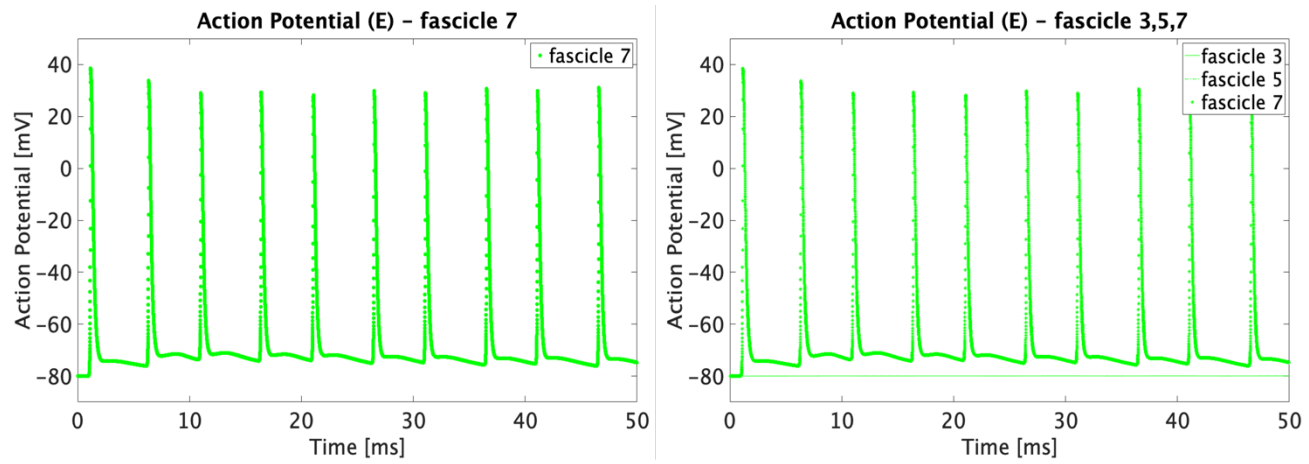

(iii)

Fig. 15 Action potentials (APs) related to the simulation with the most efficient reciprocal orientation between the ME-patch and the nerve fiber. On the left, the AP of the fascicle closest to the electrode (7), on the right the APs of fascicles 7,5,3 are presented; (i) is APs of fascicles of the configuration A; (ii) is APs of fascicles of the configuration C and "iii" is APs of fascicles of the configuration E.

4. Discussion

Among the innovative methods for the electrical stimulation of the peripheral nervous system (PNS), magnetoelectric nanoparticles-based strategies are emerging. However, given their electric signal rapid spatial decay, approaches based on a 3D polymer matrix loaded with magnetoelectric nanoparticles (MENPs) have started to be considered as promising alternatives, due to their characteristics of minimal invasiveness, high spatial resolution, and good biocompatibility. To this end, our study employed numerical simulations to evaluate the feasibility of using a 3D polymer matrix embedded with MENPs to wirelessly modulate neural responses. We conducted a comprehensive investigation on multiple scales, spanning from the nanometer to the millimeter size, eventually leading to the evaluation of the interaction of these composites with a model biological tissue.

Initially, our analysis focused on examining the electrical potential and current density profiles of different polymers at the nanometer scale, with the goal of identifying the most suitable material for an efficient nerve stimulation. In the second phase of the study, we explored the ability of millimetric composite patches to (i) generate electric fields and (ii) spark action potentials within peripheral nerve fibers, using electromagnetic simulations and neuronal modeling solver. This combined approach provides a thorough understanding of the actual interaction between the MENPs-based composite 3D electric interface and the peripheral nerve tissue used as model.

The electrical characteristics of the matrix polymer were varied to evaluate the performance of the nanometric base unit, depending on the type of material surrounding the MENPs. Three different polymer formulations were examined, ranging from synthetic materials (PCL, P3HT) to naturally-based materials (fibroin silk blend with PPy), covering a wide range of different electrical conductivity values.

PCL (polycaprolactone) is an inexpensive thermoplastic material widely used as a scaffold for cell culture and for neural tissue interfaces due to its slow degradation rate, low melting point, low melting point and solubility in various solvents [4],[25]. However, its low electrical conductivity would require additional fabrication strategies to improve it, such as mixing with other polymers or incorporating highly conductive nanomaterials. In this investigation, pristine PCL (with a conductivity of $\sigma = 10^{-6}$ S/m) serves as a negative control to evaluate the electrical behavior of the ME-Patch composite when MENPs are introduced into a low-conductivity matrix [26], [27]. Biomaterials are recognized for their enhanced biocompatibility, bioactivity and ability to biodegrade completely in a biological environment, making them more advantageous than synthetic polymers to develop tissue interfaces. In this contest, silk fibroin, a protein produced by the silkworm (*Bombyx mori*), has attracted considerable interest [28]. The presence of functional groups in the fibroin protein chain allows adhesion to tissues, chemical modification and integration with functional materials such as conductive polymers [29], expanding its applications. In this report, a composite blend of polypyrrole (PPy) and silk fibroin (SF) with a final conductivity of *80 S/m* [30] was considered, which corresponds to the intermediate level of conductivity for this case study. Lastly, P3HT, a conductive polymer widely used in various applications was analyzed [31]. Due to its relatively low cytotoxicity and good physical and chemical stability in biological environments, P3HT-based systems have also already been explored for biomedical applications [32], [33]. The conductivity of the polymer in pure form can be greatly enhanced (up to several orders of

magnitude) by chemical or electrochemical doping methods [34]. Electrochemically doped P3HT-based material [35] has been herein considered as an experimental reference to model biomaterials with a wide conductivity spectrum, ranging from the least conductive PCL ($\sigma \approx 10^{-6}$ S/m) to the most conductive P3HT ($\sigma \approx 10^{4}$ S/m). All the formulations considered in the study are recognized as biocompatible and adaptable to numerous biotechnology areas (i.e., tissue engineering, drug delivery, biosensors). Moreover, they can be quite easily processed with the most common polymers fabrication techniques, such as electrospinning, 3D printing and casting deposition.

At the nanometric level, the study delved into the electrical properties of three distinct polymers—PCL, SF-PPy, and P3HT—embedded with MENPs. Using the Sim4life modeling platform, magnetoelectric nanoparticles (MENPs) were modeled in terms of electrical characteristics only, and simulations were performed at a low stimulation frequency (100 Hz), to interact effectively with biological systems. In Fig. 7 Electrical potential distributions at the surface and in the central slice are shown, while the ME-Patch current density profiles of the three composites are reported in Fig. 8 (qualitative visualization), Table 3 (quantitative analysis), and in Fig. 9 (boxplots). Visualizing the electric potential across the surfaces of these nanocomposites provided crucial insights into their performances. Notably, the MENPs-P3HT system exhibited the highest electrical potential conductivity, closely followed by MENPs-SF-PPy, while MENPs-PCL demonstrated significantly lower potential values, nearing zero due to its extremely poor conductivity ($\sigma \approx 10^{-6}$ S/m). This disparity in electrical potential underscored the importance of polymer selection in optimizing the performance of magnetoelectric patches. Furthermore, a comprehensive assessment of the current density distribution across the surfaces of these nanocomposites provided additional insights. As expected, the MENPs-P3HT system exhibited notably higher current density values compared to MENPs-SF-PPy and MENPs-PCL. Overall, the qualitative and the statistical parameters highlighted the robust electrical performance of the MENPs-P3HT system, positioning it as the most promising candidate for further investigation.

Then, the effect of the transition from nanometer to micrometer structure is investigated. To understand how the collective behavior of multiple nanometric units influence the overall electrical performance of a larger micrometric assembly, particular attention is given to the potential distribution and the current density. In Fig. 10, the distribution of the electric potential developed at the patch after the MENPs activation in the micrometer structure is presented, followed by a statistical evaluation of such electric potential data distribution within each cube face (Table 4). We observed that the repetition in the space of the unit bases led to the formation of a "patterned" voltage arrangement. However, despite the change to larger structures, the overall dipolar behavior was maintained. In particular, the maximum values of the potential modulus of the positive and negative faces are 1.7 mV, which are slightly lower than those presented on the encapsulated MENPs (i.e., 2.25 mV); more importantly, these maximum values are constant across the three nano- and micro-assemblies under study, suggesting that such potential would be present also in larger structures (i.e., millimetric structure). Fig. 11 reports on the current density distribution to understand how it varies between the different faces of the cubic patches. By comparing the current density values between the nanometric and micrometric structures (summarized in Table 5), it is possible to notice the maintenance of the electrical performance, by increasing the ME-Patch dimension.

Thus, the micrometric structure not only kept the initial dipolar behavior, but also presented the same current density values observed in the other models (nanometric, micrometric with 165 MENP,

and micrometric with 384 MENP), demonstrating the preservation of the essential electrical characteristics despite the increase in size.

These findings provided crucial insights for proceeding with the final step of this work: the modeling of a clinically-relevant magnetoelectric biointerface. In order to model a millimetric soft patch we had to overcome the computational limitations inherent to the software/machine cluster in use, which (i) did not allow a correct/complete discretization of nanometric entities when millimetric objects are located nearby such as for the case of nanometric MENPs and a millimetric nerve, and (ii) did not sustain calculations with more than 400 MENPs. Therefore, for the millimetric model, an appropriate electrical potential (i.e., +/- 5.25 V, Fig. 12 and Table 6) is imposed on the surface of the MENPs within the millimeter cubic matrix, such as to achieve a current density distribution with similar statistical values to that observed in the nanometric structure ($J = 8.29 \times 10^7$, Table 6).

Six configurations of our millimetric ME-patch are alternatively placed in contact with a realistic nerve model and used for the electromagnetic stimulation assessment. Fig. 13 (A – B, C – D and E – F) and Fig. 14 show the electric field distributions following simulations in the nerve tissue and their spatial decay along its cross-section, respectively. This analysis shows that the electric field profile in the cross-section of the nerve changes as a response to the side of the magnetoelectric, millimeter patch that is in direct contact with it. In addition, the observed non-uniform propagation of the electric field can be ascribed to the different electrical properties of the various biological structures encountered. However, the generated electric field is higher than the threshold values required to elicit a neuronal response (100 V/m) [36], suggesting the ability of our millimetric soft electrode to act as a wireless source of electric field in the body, effectively modulate neuronal activity, and stimulate the surrounding nerve tissue.

Hence, as a final step, the neuronal dynamics of motor neurons was investigated, by coupling Sim4Life with Neuron, a solver that applies the electric field values obtained from previous electromagnetic simulations as input. For each pair, the configurations with the slowest spatial decay were evaluated (i.e., simulations A, C and E, Fig. 14).

The neuronal response is characterized by a series of action potentials (APs), which consist of several basic phases. Voltage-dependent sodium ($Na+$) and potassium ($K+$) ion channels are proteins present in the cell membrane of neurons and play a key role in the generation and transmission of nerve impulses [37]. These channels are regulated by variations in the electrical membrane potential, and they open or close in response to these changes. Initially, a resting state is observed, where the neural membrane potential is maintained around -80 mV, stabilized mainly by potassium ions permeability. When the neuron is stimulated and the membrane potential exceeds a certain threshold, the depolarization phase begins. During this phase, voltage-dependent sodium channels open, allowing rapid entry of sodium ions into the cell and causing the membrane potential to rise in order to reach the electrochemical equilibrium for sodium ions. This peak potential phase is known as overshoot. Next, the repolarization phase occurs, in which voltage-dependent potassium channels open, while sodium channels close. This leads to an efflux of potassium from the cell, restoring the membrane potential to resting values. The repolarization phase is followed by a period of hyper-polarization, during which the membrane potential becomes more negative than its resting value, before gradually returning to resting levels [38]. Throughout the process, usually it is around a few milliseconds, the refractory period of the neural membrane limits the ability to generate new

action potentials. [39]. This sequence of events represents a crucial mechanism in neuronal signal transmission and information integration in the nervous system [40].

Data analysis revealed that the typical pulses of the action potential are clearly observable in the graphs in Fig. 15. Interestingly, activation of fascicle 7 (the closest to the ME-patch) is observed in all three configurations (A, C, E), suggesting that the generation of the action potential is independent from their amplitude differences, if a certain threshold is exceeded. However, while the periodicity of the first two cases (A, C) is similar, in the last configuration (E) it is increased, suggesting possible effects due to the different refractory periods of the three stimulations. In the first ones (A and C), associated with more intense and penetrating electric fields, a reduced periodicity and a prolonged refractory period are detected. This may be due to the wider negative sinusoidal half-wave input, extending the refractory period compared to the third case (E) characterized by a less intense and more rapidly decreasing electric field. Finally, the concept of deep stimulation was further investigated. For this purpose, action potentials related to fascicles 3, 5 and 7 were plotted for the three most efficient stimulation configurations (A, C and E). Being gradually distant from the electrode, these fascicles were affected differently by the electric field generated by the ME-patch. As expected, scenarios with a more penetrating electric field or determined by values for each point above threshold (A and C) have returned AP activation in all fascicles, indicating deep stimulation. In both cases, different periodicity of the APs generated in the various fascicles under study was observed, since the stimulation sine wave perceived by the farthest ones is shallower compared to the sine wave sensed by fascicle 7; again, this could be referred to a different refractory period. On the contrary, the configuration characterized by a lower electric field distribution and thus exhibiting a very rapid electromagnetic field decay (E), presents a neuronal response only within the fascicle closest to the electrode (fascicle 7), while the other two (fascicle 5 and fascicle 3) were reached by subthreshold values, unable to generate action potentials.

5. Conclusions

A multiscale computational framework is developed and optimized in the present study for the design of a novel noninvasive wireless electrical stimulation technology capable of effectively activating a neuronal response. We developed an optimized three-dimensional nanostructured magnetoelectric patch by precisely defining the polymer matrix composition and loading concentrations of magnetoelectric nanoparticles (MENPs). This optimization step is essential for an efficient and controlled transmission of the MENPs electricity through a biocompatible wireless system, with the goal of triggering neuronal action potentials and distributing the electric field in a targeted manner within a human nerve tissue model.

Our methodological approach allowed us to accurately simulate the effectiveness of the magnetoelectric patch in generating neuronal action potentials and modulating electric field distribution. Future developments from this study include the investigation of different ME-Patch shapes/geometries, such as thinner films or grids, as well as the implementation of a patterned voltage structure, in order to (i) more faithfully replicate the behavior of a realistic material and (ii) further optimize the nerve tissue stimulation on a larger and more representative scale.

In conclusion, the outcomes of this thesis constitute a solid scientific basis for the development of advanced bioelectric-based strategies for the treatment of impaired nerve tissues, representing a significant step forward in the engineering of magnetoelectric devices for neural interfacing.

References

[1] K. S. Wuolle *et al.*, "Satisfaction with and usage of a hand neuroprosthesis," *Arch Phys Med Rehabil*, vol. 80, no. 2, pp. 206–213, Feb. 1999, doi: 10.1016/S0003-9993(99)90123-5.

[2] K. L. Kilgore, K. D. Anderson, and P. H. Peckham, "Neuroprosthesis for individuals with spinal cord injury," *Neurol Res*, vol. 45, no. 10, pp. 893–905, 2023, doi: 10.1080/01616412.2020.1798106.

[3] A. Gupta, N. Vardalakis, and F. B. Wagner, "Neuroprosthetics: from sensorimotor to cognitive disorders," *Communications Biology*, vol. 6, no. 1. Nature Research, Dec. 01, 2023. doi: 10.1038/s42003-022-04390-w.

[4] C. Marquez-Chin and M. R. Popovic, "Functional electrical stimulation therapy for restoration of motor function after spinal cord injury and stroke: A review," *BioMedical Engineering Online*, vol. 19, no. 1. BioMed Central Ltd., May 24, 2020. doi: 10.1186/s12938-020-00773-4.

[5] B. M. Doucet, A. Lam, and L. Griffin, "Focus: Biomedical Engineering neuromuscular Electrical Stimulation for Skeletal Muscle Function," 2012.

[6] S. Khizroev and P. Liang, "Engineering Future Medicines with Magnetoelectric Nanoparticles: Wirelessly controlled, targeted therapies," *IEEE Nanotechnol Mag*, vol. 14, no. 1, pp. 23–29, Feb. 2020, doi: 10.1109/MNANO.2019.2952227.

[7] R. K. Tekade, R. Maheshwari, N. Soni, M. Tekade, and M. B. Chougule, "Nanotechnology for the Development of Nanomedicine," *Nanotechnology-Based Approaches for Targeting and Delivery of Drugs and Genes*, pp. 3–61, Jan. 2017, doi: 10.1016/B978-0-12-809717-5.00001-4.

[8] S. Fiocchi, E. Chiaramello, A. Marrella, M. Bonato, M. Parazzini, and P. Ravazzani, "Modelling of magnetoelectric nanoparticles for non-invasive brain stimulation: a computational study," *J Neural Eng*, vol. 19, no. 5, Oct. 2022, doi: 10.1088/1741-2552/ac9085.

[9] A. Kumari, S. K. Yadav, and S. C. Yadav, "Biodegradable polymeric nanoparticles based drug delivery systems," *Colloids Surf B Biointerfaces*, vol. 75, no. 1, pp. 1–18, Jan. 2010, doi: 10.1016/j.colsurfb.2009.09.001.

[10] F. Mushtaq *et al.*, "Magnetoelectric 3D scaffolds for enhanced bone cell proliferation," *Appl Mater Today*, vol. 16, pp. 290–300, Sep. 2019, doi: 10.1016/J.APMT.2019.06.004.

[11] H. A. El Azim, "Magneto-electric nanocarriers for drug delivery: An overview," *J Drug Deliv Sci Technol*, vol. 37, pp. 46–50, Feb. 2017, doi: 10.1016/J.JDDST.2016.11.003.

[12] S. Fiocchi *et al.*, "Modeling of core-shell magneto-electric nanoparticles for biomedical applications: Effect of composition, dimension, and magnetic field features on magnetoelectric response," *PLoS One*, vol. 17, no. 9 September, Sep. 2022, doi: 10.1371/journal.pone.0274676.

[13] S. V Suryanarayana, "Magnetoelectric interaction phenomena in materials," 1994.

[14] H. Song, M. A. Listyawan, and J. Ryu, "Core–Shell Magnetoelectric Nanoparticles: Materials, Synthesis, Magnetoelectricity, and Applications," *Actuators*, vol. 11, no. 12. MDPI, Dec. 01, 2022. doi: 10.3390/act11120380.

[15] S. Kopyl, R. Surmenev, M. Surmeneva, Y. Fetisov, and A. Kholkin, "Magnetoelectric effect: principles and applications in biology and medicine– a review," *Materials Today Bio*, vol. 12. Elsevier B.V., Sep. 01, 2021. doi: 10.1016/j.mtbio.2021.100149.

[16] A. E. Danks, S. R. Hall, and Z. Schnepp, "The evolution of 'sol-gel' chemistry as a technique for materials synthesis," *Mater Horiz*, vol. 3, no. 2, pp. 91–112, Mar. 2016, doi: 10.1039/c5mh00260e.

[17] H. Wu, P. Xue, Y. Lu, and X. Zhu, "Microstructural, optical and magnetic characterizations of BiFeO3 multiferroic nanoparticles synthesized via a sol-gel process," *J Alloys Compd*, vol. 731, pp. 471–477, Jan. 2018, doi: 10.1016/J.JALLCOM.2017.10.087.

[18] K. Yue, R. Guduru, J. Hong, P. Liang, M. Nair, and S. Khizroev, "Magneto-Electric Nano-Particles for Non-Invasive Brain Stimulation," *PLoS One*, vol. 7, no. 9, Sep. 2012, doi: 10.1371/journal.pone.0044040.

[19] I. Takako Smith *et al.*, "Nanomedicine and nanobiotechnology applications of magnetoelectric nanoparticles," *WIREs Nanomed Nanobiotechnol*, 2023, doi: 10.1002/wnan.1849.

[20] A. Marrella *et al.*, "Magnetoelectric nanoparticles shape modulates their electrical output," *Front Bioeng Biotechnol*, vol. 11, 2023, doi: 10.3389/fbioe.2023.1219777.

[21] "References Low Frequency Conductivity_database V4.1".

[22] C. C. McIntyre, A. G. Richardson, and W. M. Grill, "Modeling the excitability of mammalian nerve fibers: Influence of afterpotentials on the recovery cycle," *J Neurophysiol*, vol. 87, no. 2, pp. 995–1006, 2002, doi: 10.1152/jn.00353.2001.

[23] J. L. Gaines, K. E. Finn, J. P. Slopsema, L. A. Heyboer, and K. H. Polasek, "A model of motor and sensory axon activation in the median nerve using surface electrical stimulation," *J Comput Neurosci*, vol. 45, no. 1, pp. 29–43, Aug. 2018, doi: 10.1007/s10827-018-0689-5.

[24] D. Mawad *et al.*, "A conducting polymer with enhanced electronic stability applied in cardiac models." [Online]. Available: https://www.science.org

[25] M. J. Mochane, T. S. Motsoeneng, E. R. Sadiku, T. C. Mokhena, and J. S. Sefadi, "Morphology and properties of electrospun PCL and its composites for medical applications: A mini review," *Applied Sciences (Switzerland)*, vol. 9, no. 11. MDPI AG, Jun. 01, 2019. doi: 10.3390/app9112205.

[26] G. Damonte, A. Vallin, A. Fina, and O. Monticelli, "On the development of an effective method to produce conductive pcl film," *Nanomaterials*, vol. 11, no. 6, Jun. 2021, doi: 10.3390/nano11061385.

[27] M. Heidari, S. H. Bahrami, M. Ranjbar-Mohammadi, and P. B. Milan, "Smart electrospun nanofibers containing PCL/gelatin/graphene oxide for application in nerve

tissue engineering," *Materials Science and Engineering C*, vol. 103, Oct. 2019, doi: 10.1016/j.msec.2019.109768.

[28] A. J. Meinel *et al.*, "Optimization strategies for electrospun silk fibroin tissue engineering scaffolds," *Biomaterials*, vol. 30, no. 17, pp. 3058–3067, Jun. 2009, doi: 10.1016/j.biomaterials.2009.01.054.

[29] W. Zhao *et al.*, "Functionalized hydrogels in neural injury repairing," *Frontiers in Neuroscience*, vol. 17. Frontiers Media SA, 2023. doi: 10.3389/fnins.2023.1199299.

[30] L. X. Liu, W. Chen, H. Bin Zhang, Q. W. Wang, F. Guan, and Z. Z. Yu, "Flexible and Multifunctional Silk Textiles with Biomimetic Leaf-Like MXene/Silver Nanowire Nanostructures for Electromagnetic Interference Shielding, Humidity Monitoring, and Self-Derived Hydrophobicity," *Adv Funct Mater*, vol. 29, no. 44, Nov. 2019, doi: 10.1002/adfm.201905197.

[31] A. Santos, P. Formentín, J. Pallarés, J. Ferré-Borrull, and L. F. Marsal, "Fabrication and characterization of high-density arrays of P3HT nanopillars on ITO/glass substrates," *Solar Energy Materials and Solar Cells*, vol. 94, no. 7, pp. 1247–1253, Jul. 2010, doi: 10.1016/J.SOLMAT.2010.03.016.

[32] S. Zhang, H. Yan, J. M. Yeh, X. Shi, and P. Zhang, "Electroactive Composite of FeCl3-Doped P3HT/PLGA with Adjustable Electrical Conductivity for Potential Application in Neural Tissue Engineering," *Macromol Biosci*, vol. 19, no. 10, Oct. 2019, doi: 10.1002/mabi.201900147.

[33] D. Ghezzi, M. R. Antognazza, M. Dal Maschio, E. Lanzarini, F. Benfenati, and G. Lanzani, "A hybrid bioorganic interface for neuronal photoactivation," *Nat Commun*, vol. 2, no. 1, 2011, doi: 10.1038/ncomms1164.

[34] S. Kesornsit *et al.*, "Synthesis of Highly Conductive Poly(3-hexylthiophene) by Chemical Oxidative Polymerization Using Surfactant Templates," *Polymers (Basel)*, vol. 14, no. 18, Sep. 2022, doi: 10.3390/polym14183860.

[35] D. Neusser, C. Malacrida, M. Kern, Y. M. Gross, J. Van Slageren, and S. Ludwigs, "High Conductivities of Disordered P3HT Films by an Electrochemical Doping Strategy," *Chemistry of Materials*, vol. 32, no. 14, pp. 6003–6013, Jul. 2020, doi: 10.1021/acs.chemmater.0c01293.

[36] N. Danner, M. Könönen, L. Säisänen, R. Laitinen, E. Mervaala, and P. Julkunen, "Effect of individual anatomy on resting motor threshold – Computed electric field as a measure of cortical excitability," *J Neurosci Methods*, vol. 203, no. 2, pp. 298–304, Jan. 2012, doi: 10.1016/J.JNEUMETH.2011.10.004.

[37] M. Heine, A. Ciuraszkiewicz, A. Voigt, J. Heck, and A. Bikbaev, "Surface dynamics of voltage-gated ion channels," *Channels*, vol. 10, no. 4. Taylor and Francis Inc., pp. 267–281, Jul. 03, 2016. doi: 10.1080/19336950.2016.1153210.

[38] C. J. Heckman and R. M. Enoka, "Physiology of the motor neuron and the motor unit," *Handbook of Clinical Neurophysiology*, vol. 4, no. C, pp. 119–147, Jan. 2004, doi: 10.1016/S1567-4231(04)04006-7.

[39] T. W. Farmer, F. Buchthal, and P. Rosenfalck, "Refractory period of human muscle after the passage of a propagated action potential," *Electroencephalogr Clin Neurophysiol*, vol. 12, no. 2, pp. 455–466, May 1960, doi: 10.1016/0013-4694(60)90021-3.

[40] J. Hounsgaard, "Motor neurons," *Compr Physiol*, vol. 7, no. 2, pp. 463–484, Apr. 2017, doi: 10.1002/cphy.c160025.

Abstract in Italiano

Le nanoparticelle magnetoelettriche (MENPs) possono generare campi elettrici locali elevati se attivate con campi magnetici di bassa intensità. Tuttavia, quando vengono somministrate singolarmente, le MENP possono essere posizionate in modo casuale e tendono a formare dei cluster. I campi elettrici indotti che ne derivano decadono molto rapidamente all'aumentare della distanza, compromettendo un'efficace stimolazione dei tessuti. In questo contesto, il seguente studio introduce un nuovo approccio per la stimolazione dei tessuti che impiega nanoparticelle magnetoelettriche incorporate in una matrice polimerica 3D biocompatibile (ME-Patch). Attraverso un approccio in silico, le prestazioni elettriche del ME-Patch vengono ottimizzate, a partire dall'implementazione di una modellazione su scala nanometrica in cui vengono accuratamente studiati i comportamenti elettrici dei materiali, fino a raggiungere la valutazione funzionale del patch con un modello realistico di nervo periferico. I nostri risultati offrono spunti per la fabbricazione di dispositivi magnetoelettrici soft e biocompatibili in grado di immagazzinare e trasferire gli effetti delle MENP per innescare potenziali d'azione neuronali. Sfruttando la capacità di tali nanosorgenti di generare elettricità in modalità wireless come risposta a campi magnetici a bassa intensità, il nostro approccio promette una stimolazione nervosa non invasiva, superando le numerose limitazioni associate agli stimolatori convenzionali e presentando interessanti opportunità per l'avanzamento delle tecnologie di interfacciamento neurale.